INVESTIGATION OF VORTEX FORMATION IN THE VICINITY OF PARALLEL PLATES IN OSCILLATING FLOW USING PARTICLE IMAGE VELOCIMETRY

M. Rezk, A.H. Ibrahim[1], T. Nigim, A. I. Abd El-Rahman[1], A.A. Elbeltagy and Ehab Abdel-Rahman[+]

School of Sciences and Engineering, American University in Cairo
11835 New Cairo, Egypt
[+] Corresponding author: ehab_ab@aucegypt.edu

Oscillating flows differ significantly from steady flows in many terms including onset of turbulence, flow morphology, amount of turbulence and heat transfer characteristics during sudden expansion and contraction. This work uses Particle Image Velocimetry measurements to capture the vortex generation and flow morphology at the edges of a set of parallel plates in an oscillating flow driven by an electrodynamic loudspeaker inside a thermoacoustic resonator. The current work investigates the temporal development of the vortex at different points along the acoustic cycle, examines the effects of plate thickness, plate separation and drive ratio on the flow morphology around the stack edge. This is of particular interest to thermoacoustic engines and refrigerators where the vortex structures generated at the inlets and exits of thermoacoustic stacks play a role in the non-linear losses that dissipate flow energy into heat and thus degrade the performance. The work presents measured velocity field for different cases. Results visualize and quantify how the vortex size and the size of the disturbance zone increase with the plate thickness and how the size of vortex-vortex interaction along the same plate or between two different plates decreases. Increasing the plate separation does not seem to affect the vortex size nor the size of the disturbance zone but it reduces the vortex-vortex interaction along the same plate. Increasing the drive ratio increases the vortex size, the vortex-vortex interaction and the size of the disturbance zone and greatly affects the dissipation of flow energy into heat. This work visualizes and quantifies these effects for a range of values of dimensionless numbers.

1 Introduction

Oscillating flows of near-zero mean differ significantly from steady flows. Limited work has been made to identify onset of turbulence, vortex generation, entrance length, and flow morphology and heat transfer characteristics [1] [2] [3] [4]. For example, Peacock and Stairmand [5] reported that laminar oscillating flows have shorter entrance length than in straight flows which impacts the development of the flow. These differences are very critical during sudden contraction or expansion as encountered during entrance and exit of stack pores in thermoacoustic engines or refrigerators because the consequent flow separation dissipates flow energy into heat.

The disturbance caused when a flow passes around an obstacle, especially a circular cylinder, is well understood in steady flows where vorticity is created close to the cylinder surface due to the no-

[1] On leave from Mechanical Power Department, Faculty of Engineering, Cairo University, Giza, Egypt

slip boundary condition. The flow does not experience disturbance in creeping flows (Re <1). As the Reynolds number increases, twin vortices appear (4<Re<40), followed by a vortex street (40<Re<200), and flow instability (Re>200), before turbulent characteristics become dominant (Re>5000).

The flow morphology in oscillating flow is certainly less understood than in steady flows, particularly for the multi-plates forming the stacks used in thermoacoustic devices. The plate thickness and plate separation should be optimized to reduce the blockage made to the flow and to maximize the heat-transfer zone and minimize the viscous dissipation zone for the working fluid used.

Several investigations are made on the flow morphology around a single cylinder in an oscillating flow [6] or around a set of plates in an oscillatory flow. Jaworski *et al.* used Particle Image Velocimetry (PIV) to study the flow morphology around the stack edges [7]. Aben *et al.* studied the influence of different stack parameters and stack edge shapes on the generated vortex structures [8]. Berson *et al.* used PIV to study the formation of vortex structures at the edge of stacks at different plate thicknesses, plate spacings, number of plates and operating frequency [9]. Mao *et al.* developed an experimental setup using PIV to visualize the flow inside a parallel plate stack's channels [10]. Shi *et al.* studied several vortex wake patterns occurring at the end of a parallel plate stack and categorized them into eight wake patterns according to the wake morphology [11].

An important aspect in the operation of thermoacoustic refrigerators is the drive ratio, defined as the ratio of dynamic pressure amplitude to the average mean pressure. Operation at low drive ratios complies with the linear theory presented by Rott [12] and Swift [13]. Operation at higher drive ratios should generate more refrigeration power if non-linearities are controlled. Non-linear effects take the forms of turbulence, vortex formation, streaming, and generation of harmonics and these effects essentially reduce the performance of the thermoacoustics devices and thus should be deeply understood and reduced.

Several non-dimensional numbers typically are used to describe dimensionally-similar cases. The most important numbers are described here: The Reynolds number, (Re); The Strouhal number (St); and the Womersley number (Wo). The Reynolds number is defined as $\frac{VD}{\nu}$, where V is a velocity scale, D is a length scale and ν is the kinematic viscosity. The Strouhal number is defined as $\frac{fD}{V}$ where f is the operational frequency and the Womersley number as $\sqrt{Re.St}$. In this work, the length scale D is the plate separation, the velocity scale is the average velocity at a point 6.5 mm away from the stack edge. The Keulegan-Carpenter number, defined as $\frac{V}{\omega L}$, where ω is the angular oscillation frequency and L is the plate length, presents the ratio of the displacement amplitude $\frac{V}{\omega}$ to the stack length L. This particular number describes the significance of the stack end effects such that the two sides of the stack do not interact with each other for low values of the Keulegan-Carpenter number because the gas parcel displacement is much less then the plate length.

The current work uses PIV measurements to visualize the vortex generation at the edges of a set of parallel plates in an oscillating flow driven by a loudspeaker inside a thermoacoustic resonator. The current work studies the effects of plate thickness, plate separation and drive ratio on the flow morphology at the edge of parallel plate stacks. This is of particular interest to thermoacoustic engines and refrigerators where the vortex generated at the inlets and exits of thermoacoustic stacks play a role in the non-linear losses that dissipate flow energy into heat. The range of Reynolds number, Strouhal number, Womersley and Keulegan-Carpenter numbers used in this work are 8 to 280, 0.3 to 8, 8 to 17, and 0.006 to 0.207 respectively. The low Reynolds and Womersley numbers indicate that the flow is far from turbulence, the Strouhal number describes the vortex shedding from the stack while the low Keulegan-Carpenter number indicates that the plate length is much longer than gas parcel displacement meaning that the two sides of the stack do not see each others.

2 Experimental setup

A quartz thermoacoustic resonator (615 mm in length, 48 mm × 48 mm inner cross section) houses a standing wave generated using an electrodynamic commercial loudspeaker (Pioneer TS-G1013R, maximum power rating of 110 W, rated power of 20 W). The loudspeaker is placed inside an enclosure volume

(265 mm × 240 mm × 230 mm, made of glass), as shown in Figure 1.

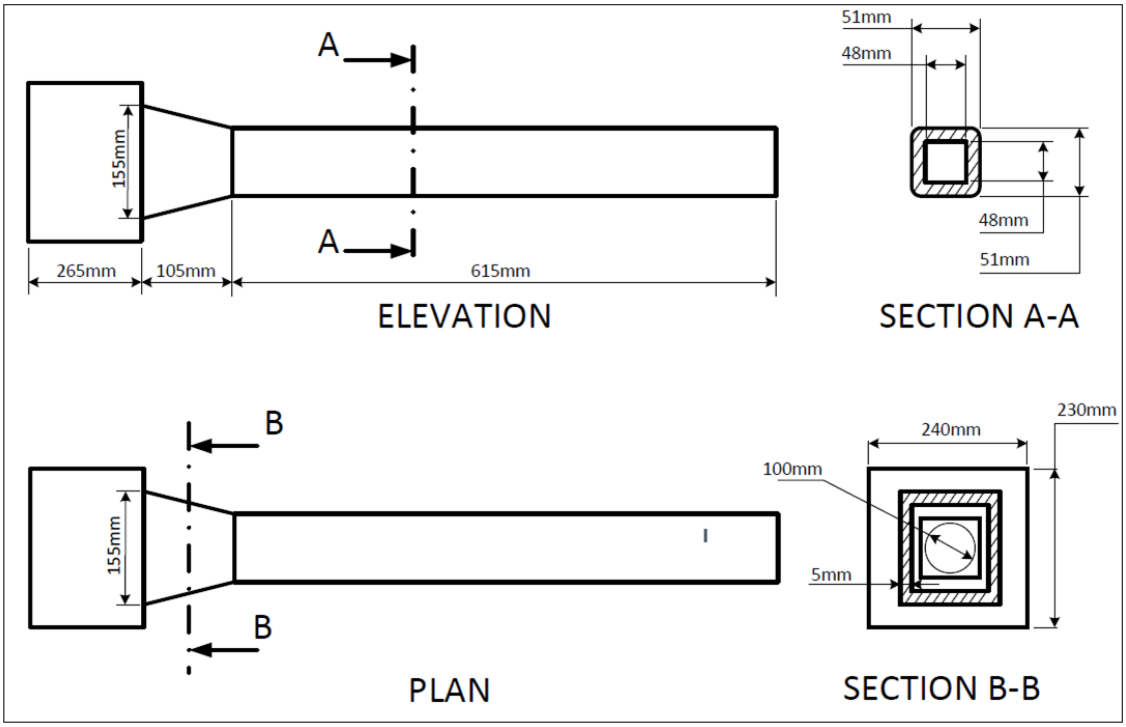

Figure 1: Schematic of the thermoacoustic resonator.

The loudspeaker is driven by a power amplifier (B & K Amplifier Type 2743) connected to a function generator (Tektronix AFG 3021B). In this configuration, the speaker is able to generate a standing wave of drive ratio up to 1.92 %.

The acoustic flow generated from the loudspeaker passes parallel to a set of plates. In this work, three different sets of plates are used to provide different plate thicknesses and different plate separations.

The first set has four plates (plate thickness of 7 mm, plate separation of 3 mm and plate length of 9 cm), the second set has three plates (plate thickness of 7 mm, plate separation of 6 mm and plate length of 9 cm), and the third set has four plates (plate thickness of 4 mm, plate separation of 6 mm and plate length of 8 cm).

In order to visualize the flow pattern around the plates, (PIV) is used. The laser light sheet is generated using a Litron Class 4 Nd:YLF laser (527 nm wavelength, supplied by Dantec Dynamics model LDY 303-PIV) and is directed normal to the resonator wall to lighten a horizontal plan in the middle of the resonator. Two consecutive PIV frames separated by 185 μs are taken repetitively at a rate of 2700 pairs per second using a CCD camera (Photron SA1.1, maximum frame rate of 5400 frames/s, a resolution of 1024×1024 Pixels^2, a pixel depth value of 12, connected to a 60 mm Nikon AF macro prime lens and housed on a 3-D mechanism). A National Instruments timer box of (Model number 80N77) is used to synchronization the laser light pulses and the CCD camera. The captured images are analyzed using the adaptive correlation technique in the software Dynamic Studio (version 2.3, supplied by Dantec Dynamics). Titanium dioxide particles (0.4 micrometer in diameter, 4000 kg/m^3, supplied by Du Pont) are used as seeding particles introduced to the resonator via a home-made seeder of a converging-diverging nozzle connected to an air-step.

The resonator is opened regularly every three to four runs to clean deposits from the seeds. Black tape is used to reduce laser glare. Figure 2 shows a schematic of the experimental setup.

Prior to measuring the flow structures around the plates in different flow configurations, PIV is used to measure the gas parcel velocity along the resonator axis and the measurements are compared to DeltaEC simulations. These measurements are made for validation purpose with no stack or plates in-

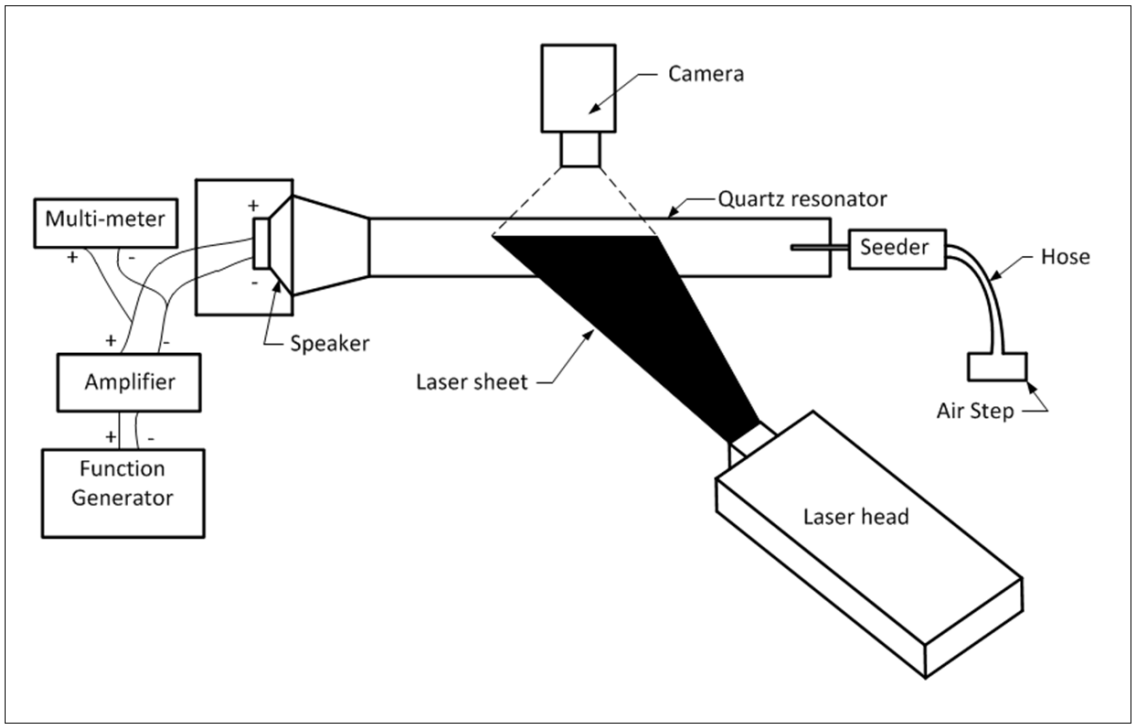

Figure 2: Schematic for the experimental setup.

side the resonator. During this process, the resonator is operated at its acoustic resonance frequency (129 Hz) and the speaker is tested in the lab to determine its mechanical resonance frequency, effective cone area, DC resistance, Bl-product, lumped stiffness and lumped mass, and mechanical resistance prior to the PIV measurements in order to properly model its performance using DeltaEC.

3 Results and discussion

This section describes the main results of this work. First, the measured gas parcel velocities around the stack are validated and the validation results are presented in section 3.1. Then, the development of the vortex structure with respect to the acoustic cycle in and out of the parallel plates is analyzed in subsection 3.2. The effects of different plate thicknesses are presented in subsection 3.3, those of different plate separations are presented in subsection 3.4 and the effects of different drive ratios are presented in subsection 3.5

3.1 Validation

For the sake of validation, gas parcel velocity is measured using PIV at different points across the length of the resonator when no stack is placed inside the resonator. The resonator is driven with a drive ratio of 0.73% at 129 Hz. The PIV system is used to measure temporal gas parcel velocity at several locations along the length of the resonator and to identify the dynamic pressure amplitude. At each measurement location 2728 images (of two-frames each separated by 185 μs) are taken at a rate of 2700 Hz giving a total measurement period of about one second. This laser triggering rate at the resonance acoustic frequency used results in about 21 points per acoustic cycle. The field of view observed by the CCD camera is 31 × 31 mm^2. Adaptive correlation technique is used to analyze the raw images and produce vector maps using a 128×128 Pixels^2 interrogation area and a moving average filter. Numerical results are computed using DeltaEC software. The comparison between the experimental and DeltaEC results

are presented in Figure 3. This result is considered a reasonable agreement and thus the work proceeds to measuring gas parcel velocities around the stack edges.

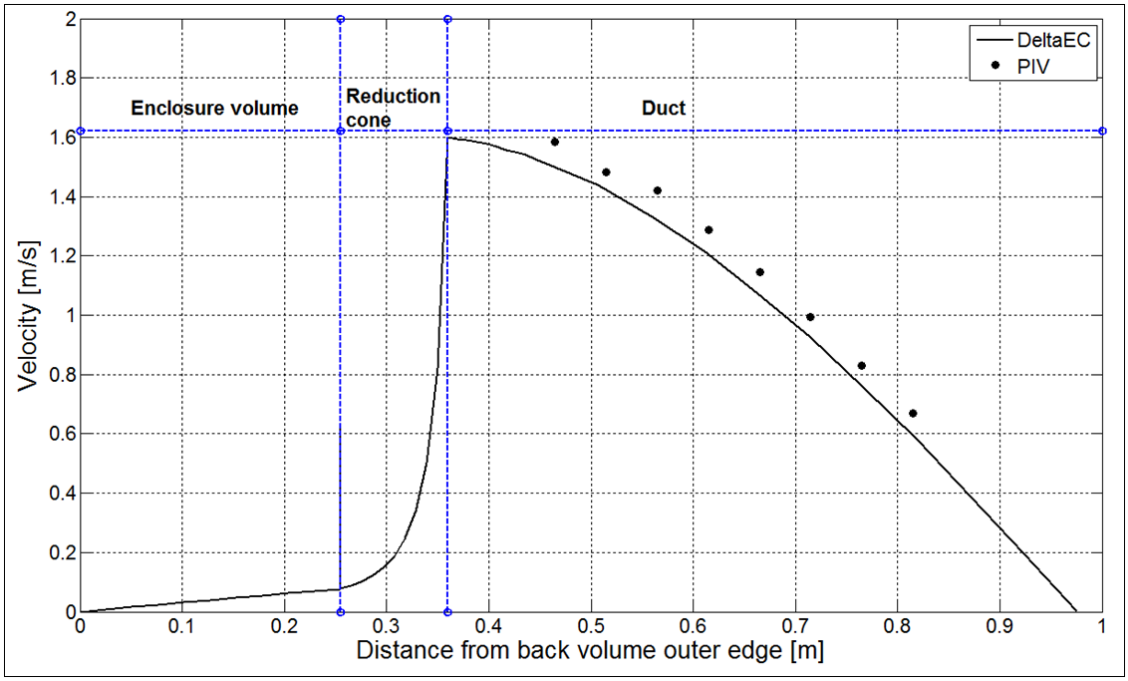

Figure 3: Measured and DeltaEC simulations for the gas parcel velocity distribution in an empty resonator at a drive ratio of 0.73%.

3.2 Temporal development of vortex structure with respect to free-stream velocity

The temporal behaviour of the vortex structure is studied at eight points along the acoustic cycle. Figure 4 shows the averaged value of velocity versus time which shows the sinusoidal acoustic velocity generated by the loudspeaker. The configuration used is a stack of four plates of 7 mm thickness each, 3 mm plate separation and 9 cm plate length.

The vortex experiences a large centrifugal force that forces the seeding particles outside of the vortex core and thus the vortex core appears as a black dot in the raw PIV images and appear with no correlation vectors in the vector maps. Guiding visual aids are used to highlight the vortex position in all the vector maps and white arrows are used to point to the black dots representing the vortex core in the raw PIV images. The values of the mean acoustic velocity 6.5 mm away from the stack edge, the Reynolds number, the Strouhal number, the Womersley number and the Keulegan–Carpenter number are stated below each figure.

The acoustic cycle consists of two halves: The first half is when the acoustic mean velocity is in the positive direction (main acoustic flow is moving towards the stack) and is represented by points A, B, C and D.

At the beginning of this part (point A), the acoustic mean velocity is very low because the flow has just experienced flow reversal and the mean kinetic energy in the flow cannot prevent flow separation when the flow experiences sudden contraction at the stack edge. Flow separation at the stack edge occurs and a vortex is formed and can be observed clearly at the stack edge in the raw PIV image and in the corresponding vector map.

As the acoustic mean velocity increases during the remaining part of this half, the mean kinetic energy of the flow increases while the vortex is pulled between the two plates into the stack away from the stack edge. Both effects reduce the vortex size and intensity and the vortex at the stack edge becomes weaker (point D for example).

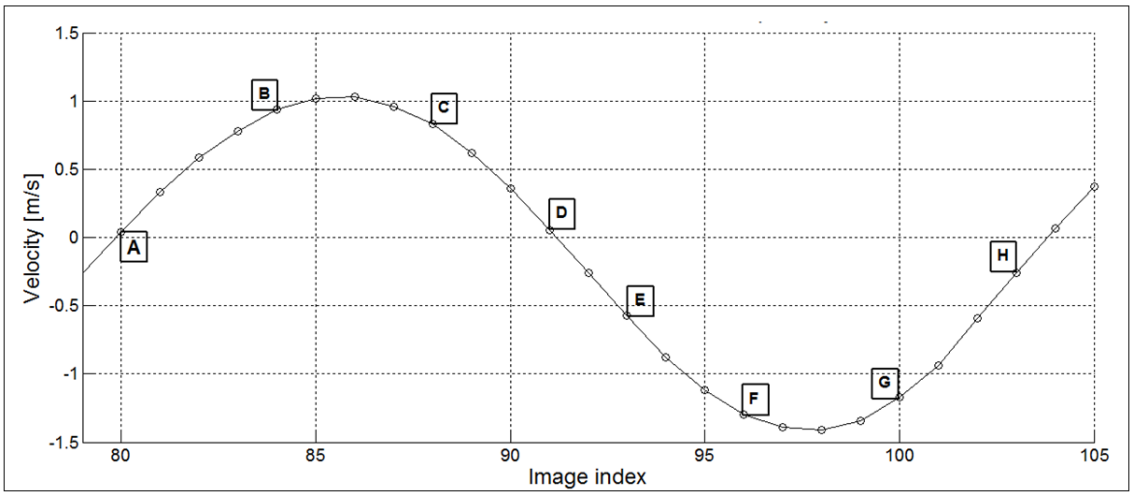

Figure 4: The acoustic cycle in the thermoacoustic device as captured by PIV for the stack configuration of 7 mm thickness and 3 mm separation away from the disturbance zone.

At the end of this half and the beginning of the second half of the acoustic cycle, the flow reverses its direction, but the flow reversal occurs inside the stack where no sudden contraction or expansion occurs and no significant disturbances are observed at the stack edge (points D and E).

During the second part of the acoustic cycle, the acoustic mean velocity is in the negative direction (main acoustic flow is moving away from the stack towards the stack edge). Points E, F, G and H present this part of the cycle. The vortex is formed again when the mean acoustic flow is about to exit the stack due to sudden expansion (point H) and the vortex core can be observed clearly at the stack edge. Then, the cycle repeats itself again.

Critical to this process is the ratio of the gas parcel displacement to the plate length (Keulegan-Carpenter number). For low Keulegan-Carpenter numbers, the stack plate is long enough with respect to the gas parcel displacement such that the two sides of the stack do not see each other. The largest Keulegan-Carpenter number used in this work is 0.2.
In summary, the peak vortex size and the largest disturbance zone occur when the flow temporally is experiencing flow reversal and the disturbance is initiated due to sudden contraction/expansion at the stack edge. The size of the disturbance zone caused by the vortex structure and to how far this disturbance zone reaches far away from the stack increases with the drive ratio and with the plate thickness and is not affected much by the plate separation.

3.3 Effects of plate thickness

This subsection describes the effect of plate thickness on the flow morphology around the stack. Two stack configurations are used: The first has three plates of 7 mm thickness each and 6 mm plate separation, and the second has four plates of 4 mm thickness each and 6 mm plate separation. The drive ratio is nearly 0.73%. Slight difference in drive ratio between the two stack configurations occur due to the difference in porosity between the two cases. The results are shown in Figure 7.

Increasing the plate thickness causes the sudden change in geometry around the plate to be more pronounced and thus the vortex size and intensity increase with the plate thickness. This can be observed through the size of the black circle where the centrifugal force pulls the seeding particles out. In the mean time, increasing the plate thickness reduces the vortex-vortex interaction that occurs along the wall of the same plate.

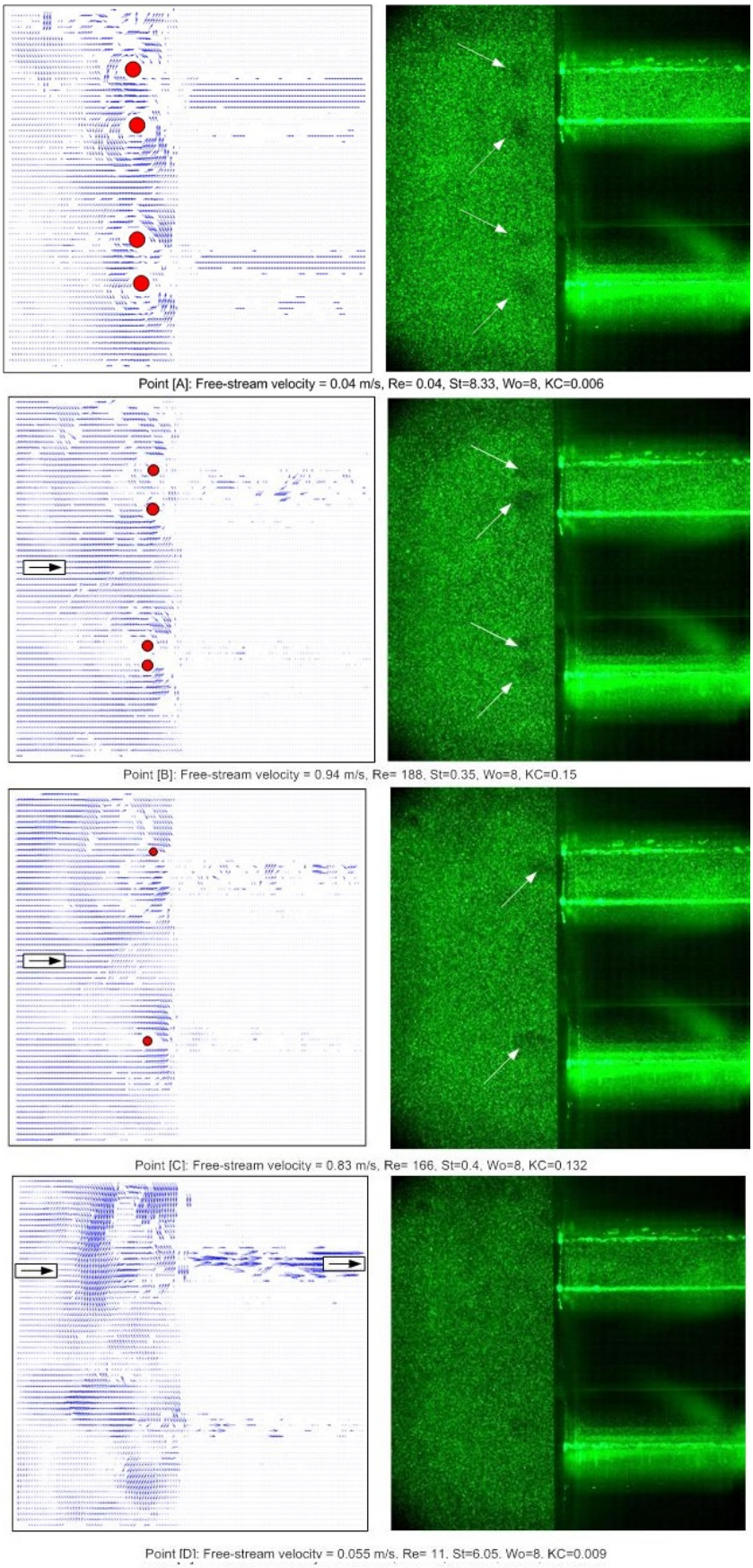

Figure 5: Points A through D on the acoustic cycle: The stack configuration is made of four plates of 7 mm plate thickness and 3 mm plate separation. The vector map of velocity (left) and the raw PIV image (right).

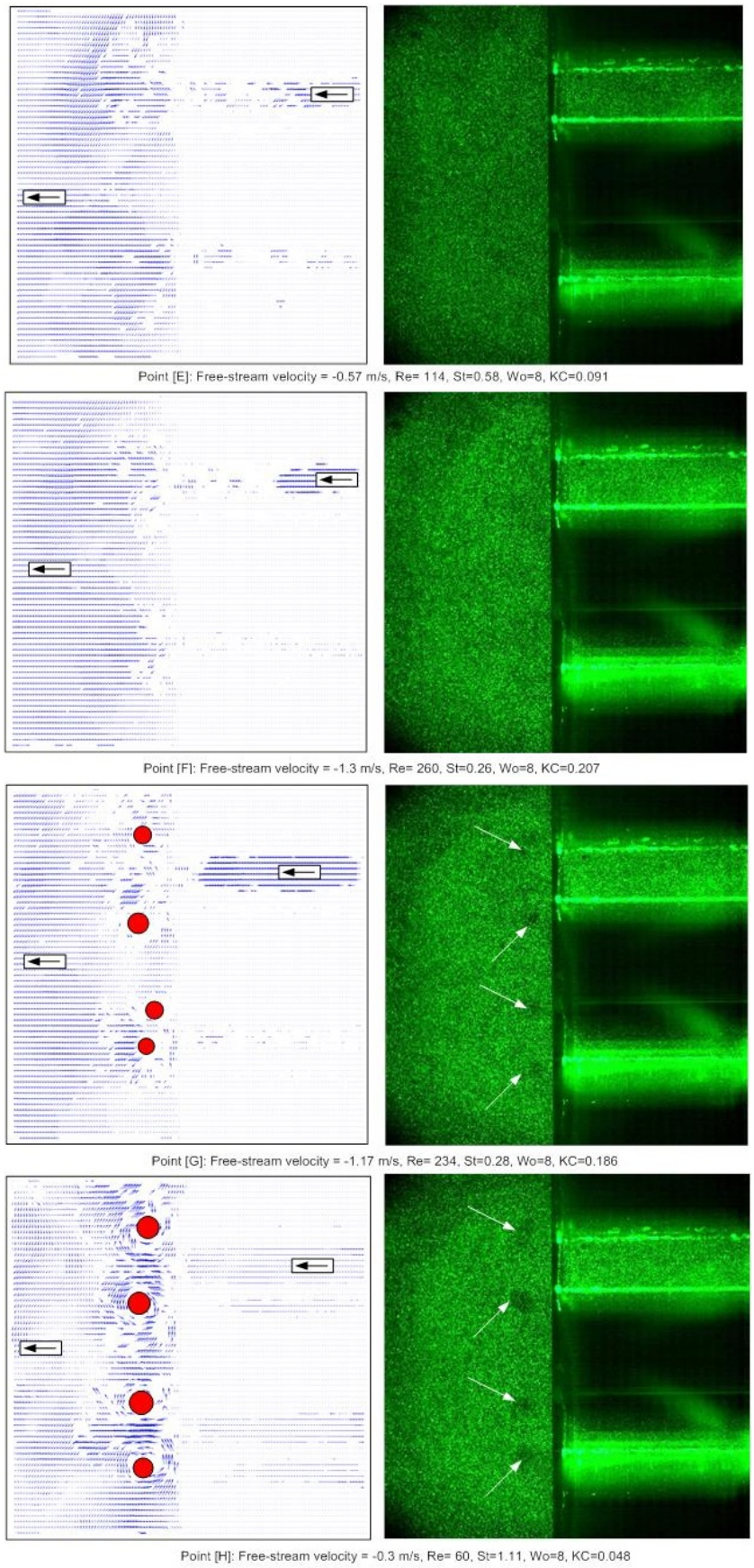

Figure 6: Point E through H on the acoustic cycle: Same stack configuration as in Figure 5.

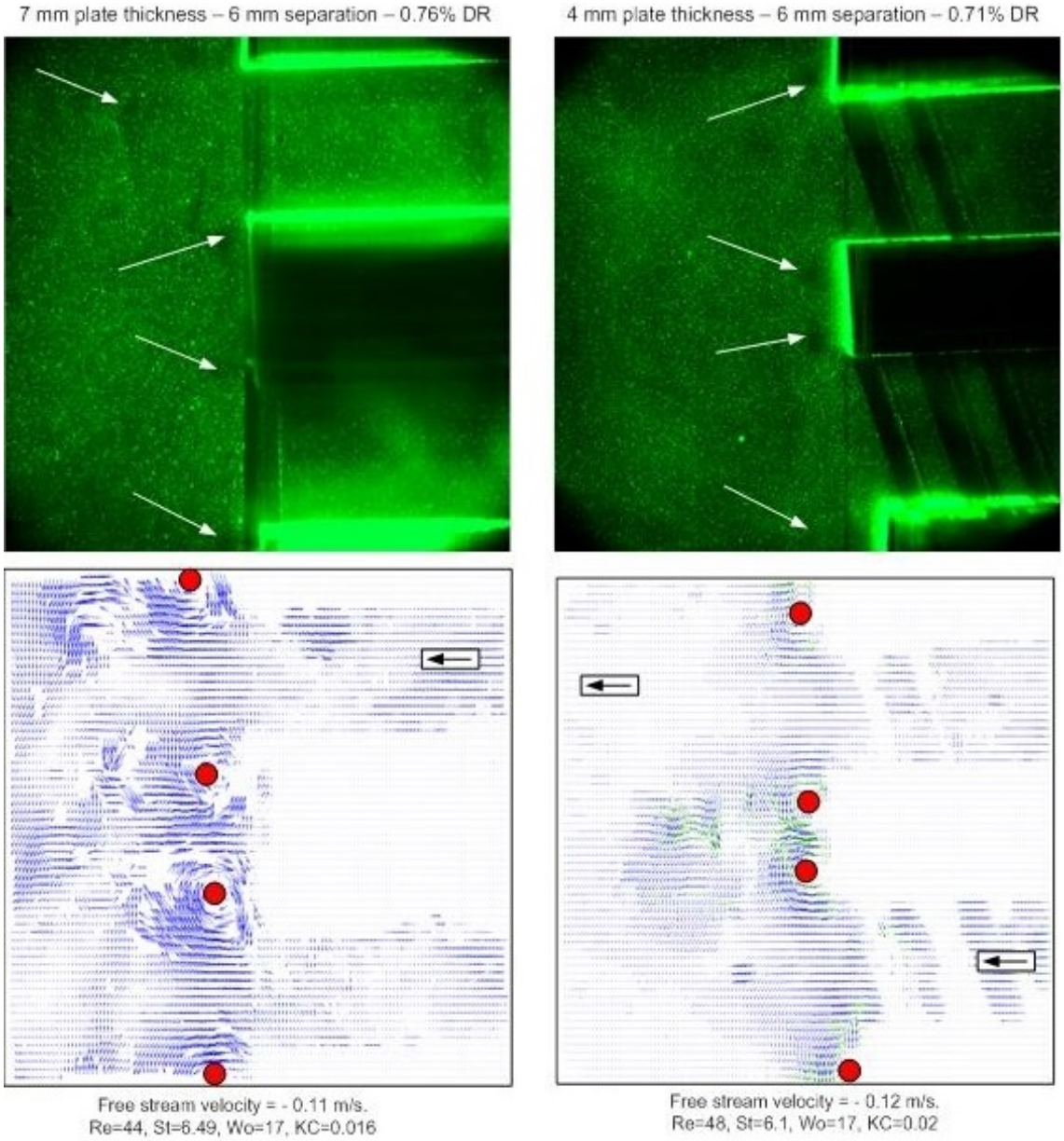

Figure 7: Effect of plate thickness on the flow morphology around the stack edge. Two plate thicknesses are used (7 mm and 4 mm) with a plate separation of 6 mm and about 0.73% drive ratio in each case. Raw PIV image (top) and vector map of velocity (bottom).

3.4 Effects of plate separation

This subsection describes the effect of plate separation on the flow morphology around the stack. Two stack configurations are used: The first has four plates of 7 mm thickness each and 3 mm plate separation, and the second has three plates of 7 mm thickness each and 6 mm plate separation. The drive ratio is nearly 0.73%. Slight difference in drive ratio between the two stack configurations occur due to the difference in porosity between the two cases. The results are shown in Figure 8.

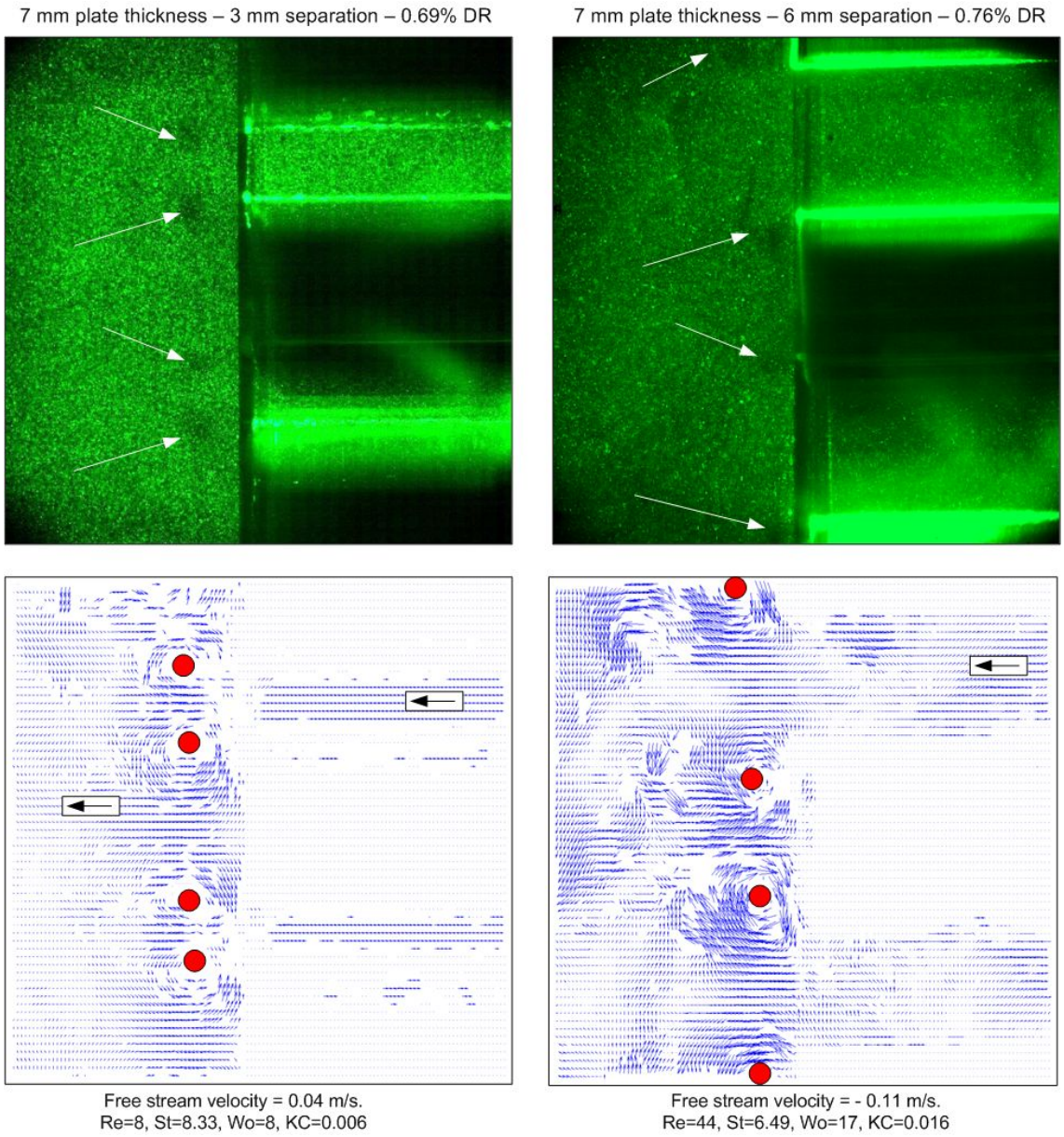

Figure 8: Effect of plate separation on the flow morphology around the stack edge. Two plate separations are used (3 mm and 6 mm) with a plate thickness of 7 mm and about 0.73% drive ratio in each case. Raw PIV image (top) and vector map of velocity (bottom).

Increasing the plate separation reduces the vortex-vortex interaction along the walls of different plates and thus reduces the overall size of the disturbance zone. At large plate separation, the two vortices that form along the walls of different plates are separated from each other and can be identified

separately. At small separation the two vortices strongly interact with each other giving rise to more complicated flow morphology.

3.5 Effects of drive ratio

This subsection describes the effect of drive ratio on the flow morphology around the stack. Two drive ratios are used, namely 0.76% (right part of Figure 8) and 1.82% (Figure 9). These drive ratios are applied to the stack configuration made of three plates of 7 mm thickness each and 6 mm plate separation. The comparison shows how increasing the drive ratio increases the size of the vortex core, the vortex-vortex interactions along the wall of the same plate or between two different vortices, increases the size of the disturbance zone, and greatly dissipates the flow energy into heat thus reducing the overall coefficient of performance of the thermoacoustic refrigerator.

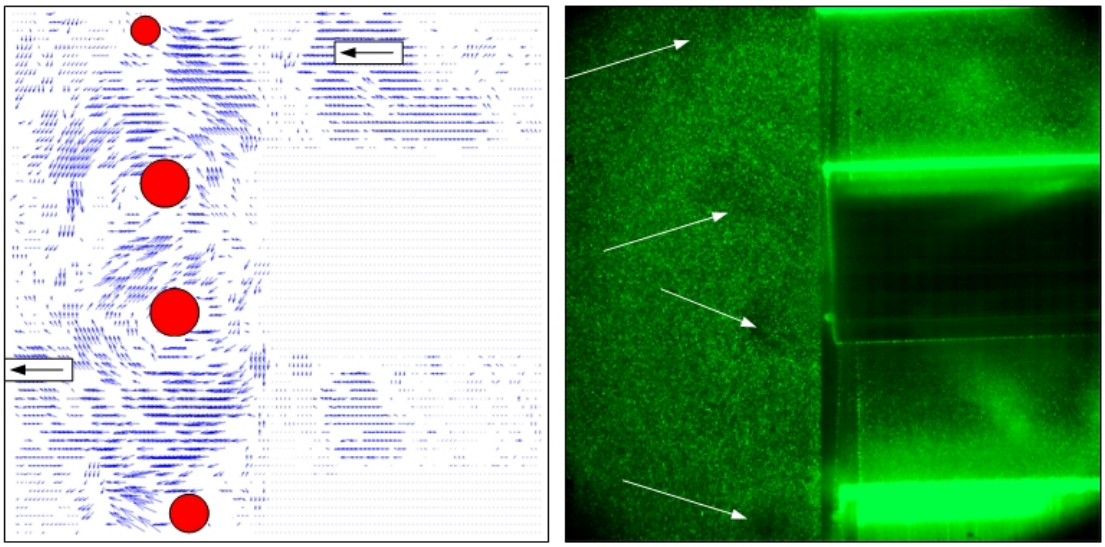

Figure 9: Flow morphology at a drive ratio of 1.82% for a stack configuration of three plates of 7 mm plate thickness and 6 mm plate separation. Vector map of velocity (left) and raw PIV image (right).

4 Summary and conclusions

The thermoacoustic device is operated with a set of parallel plates of different plate thicknesses and plate separations and at different drive ratios in order to visualize, using PIV, the flow morphology at the stack edges. The temporal development of the vortex at different points along the acoustic cycle is presented and analyzed. The effects of plate thickness, plate separation and drive ratio on the size of the vortex core, the size of the disturbance zone away from the stack, and the vortex-vortex interactions are presented and analyzed. The work visualizes and quantifies the above effects. Comparisons with computational Fluid Dynamic simulations currently are in progress.

References

[1] M. Hino, M. Kashiwayangi, M. Nakayama, and T. Hara. Experiments on the turbulence statistics and the structure of a reciprocating oscillating flow. *Journal of Fluid Mechanics*, 131:363–399, 1983.

[2] P. Merkli and H. Thomann. Transition to turbulence in oscillating pipe flow. *Journal of Fluid Mechanics*, 68:567–576, 1975.

[3] S. I. Sergeev. Fluid oscillations in pipes at moderate reynolds numbers. *Fluid Dynamics*, 1(1):121–122, 1966.

[4] R. Akhavan, R. D. Kamm, and A. H. Shapiro. An investigation of transition to turbulence in bounded oscillatory stokes flows. *Journal of Fluid Mechanics*, 131:423–444, 1983.

[5] J. A. Peacock and J. W. Stairmand. Film gauge calibration in oscillatory pipe flow. *Journal of Physics Education: Scientific Instruments*, 16:571–576, 1983.

[6] D. Nehari, V. Armenio, F. Ballio, and L. Adjlout. A 3d investigation of the dynamic loads over an array of in-line cylinders at low {KC} and re numbers. *Ocean Engineering*, 31(11–12):1503 – 1535, 2004.

[7] A. Jaworski, X. Mao, X. Mao, and Z. Yu. Entrance effects in the channels of the parallel plate stack in oscillatory flow conditions. *Experimental Thermal and Fluid Science*, 33:495–502, 2009.

[8] P.C.H. Aben, P.R. Bloemen, and J.C.H. Zeegers. 2-d piv measurements of oscillatory flow around parallel plates. *Experiments in Fluids*, 46(4):631–641, 2009.

[9] Arganthaël Berson, Marc Michard, and Philippe Blanc-Benon. Measurement of acoustic velocity in the stack of a thermoacoustic refrigerator using particle image velocimetry. *Heat and Mass Transfer*, 44(8):1015–1023, 2008.

[10] Xiaoan Mao, Zhibin Yu, ArturJ. Jaworski, and David Marx. Piv studies of coherent structures generated at the end of a stack of parallel plates in a standing wave acoustic field. *Experiments in Fluids*, 45(5):833–846, 2008.

[11] Lei Shi, Zhibin Yu, and Artur J. Jaworski. Vortex shedding flow patterns and their transitions in oscillatory flows past parallel-plate thermoacoustic stacks. *Experimental Thermal and Fluid Science*, 34(7):954 – 965, 2010.

[12] N. Rott. Thermoacoustics. *Advances in Applied Mechanics*, 20:135 – 175, 1980.

[13] G. Swift. *Thermoacoustics: A unifying perspective for some engines and refrigerators*. Acoustical Society of America, 2001.